Examination of changes to the spatial structure of turbulent boundary layers due to surface-wave forcing using POD

Owen Williams* **and Maius Wong**

Department of Aeronautics and Astronautics
University of Washington
Seattle, WA 98195
*Corresponding author: ojhw@aa.washington.edu

ABSTRACT

Changes to the spatial structure of turbulent boundary layers due to the presence free-surface waves are investigated using Partial orthogonal decomposition (POD). For the current study, the wavelength of the surface waves is approximately three times the boundary layer thickness. Large particle image velocimetry (PIV) datasets are used to obtain a wide range of converged POD modes, both with and without surface wave forcing, allowing the comparison of spatial structure. A hierarchical series of inclined low- and high-momentum structures that contribute to negative turbulent shear stress, and are reminiscent of hairpin packets, are observed near to the wall in the unperturbed case. These structures are observed to be highly disrupted by the depth-varying wave perturbation, with fewer and weaker inclined near-wall structures observed in the later case. Perhaps most significantly, all of the remaining inclined attached structures have streamwise lengthscales less than the wavelength of the disturbance and have increased angle of inclination. These results suggest that surface waves significantly alter the structure of large-scale turbulent packets with streamwise lengthscales greater or equal to the wavelength but have less effect on smaller scale productive motions.

INTRODUCTION

A detailed understanding of turbulence and mixing processes is critical to our ability to predict the onset of algal blooms (both harmful and benign) and assess human impacts on estuarine and river ecosystems. In many cases currents create a bottom boundary layer, which interacts with the free-surface and waves to heavily influence sediment/nutrient transport and dispersion of pollutants. The interaction of turbulent eddies and waves also creates an unsteady loading on tidal and river turbines that must be correctly understood to prevent damage and maximize power extraction.

Wave-boundary layer interactions have been found to cause significant changes to both mean and turbulent velocity profiles (Kemp & Simons, 1982, 1983; Borue *et al.*, 1995; Umeyama, 2005), with regions of inverted mean velocity curvature in the outer layer and reversed flow near the wall that suggest significant alterations to turbulent structure, production and transport mechanisms that may be difficult to to model using conventional assumptions. Additional complications arise from the generation of turbulent kinetic energy (TKE) by the free-surface, even in the absence of waves (Calmet & Magnaudet, 2003), and the variable orientation of wave trajectories and boundary layer currents. Depending on the distance of the BL from the free surface as well as the wave conditions, the effect of wave perturbations on submerged BLs can span the full gamut of perturbed TBL complexity as defined by Smits & Wood (1985), from the weakest case where the perturbation is gradual and obeys conventional scaling laws, to very severe, for which the flow no longer resembles a conventional turbulent boundary layer.

Previous experimental studies have examined single-point velocity measurements, often employing a triple decomposition into mean, periodic and turbulent components (Hussain & Reynolds, 1970). While this method has provided a useful statistical picture of the influence of wave-induced motions on turbulent boundary layers, these results do not allow the identification of secondary motions or provide more mechanistic explanations for changes to the spatial structure of the turbulence.

To examine changes in spatial structure, and to more accurately isolate the non-turbulent contributions to velocity statistics that are not purely sinusoidal, we employ snapshot Partial Orthogonal Decomposition (POD) (Sirovich, 1987; Holmes *et al.*, 1998). This method decomposes the flow into a set of linear orthogonal modes that are weighted by their contribution to the turbulent kinetic energy. As such, each mode provides a spatial picture of turbulent structure. The largest and most energetic modes are the fastest to converge, with higher order modes requiring more data. Given sufficient convergence, these modes appear in pairs, out of phase with each other in the streamwise direction. Given sufficient snapshots and streamwise field-of-view, alternating lobes of high and low momentum fluid, which are attached to the wall and inclined to the streamwise direction have been identified in wall-bounded flows using POD (Hellström *et al.*, 2015). Such structures are reminiscent of the structure of hairpin packets and have been shown to contribute to a majority of of the turbulent shear stress and hence turbulent production. These structures have also recently been shown to be self-similar (Hellström *et al.*, 2016). As a result POD has emerged as a very useful tool for the identification of the large-scale, productive motions in wall-bounded flows and can be used to probe the mechanistic underpinnings of the turbulent dynamics. The application of this method to the study of unsteady perturbations such as free-surface waves would serve two purposes, allowing the identification and characterization of traveling wave modes associated with the forcing and simultaneously allowing for the identification of any changes to large-scale turbulent structure.

In this study, Particle Image Velocimetry (PIV) is used to acquire large velocity-field datasets within the Air-Sea interaction flume at the University of Washington. We employ a method of randomized-sampling snapshot POD to analyze these datasets of up to 75000 snapshots, needed to ensure mode convergence in highly turbulent flow. This method has the advantage of providing highly accurate and converged approximations to the most energetic modes efficiently, instead of calculating all modes at once. The modal structure of the boundary layer, with and without waves is examined. It is demonstrated that the surface waves disrupt near-wall attached structures. Those with streamwise lengthscales smaller than the wavelength are weaker and have a greater inclination, whereas those with a lengthscale equal or greater than the wavelength are no longer observed in the presence of surface-wave disturbances.

EXPERIMENTAL SETUP

Experiments were conducted within the newly reconstructed Air-Sea Interaction facility at the University of Washington (for-

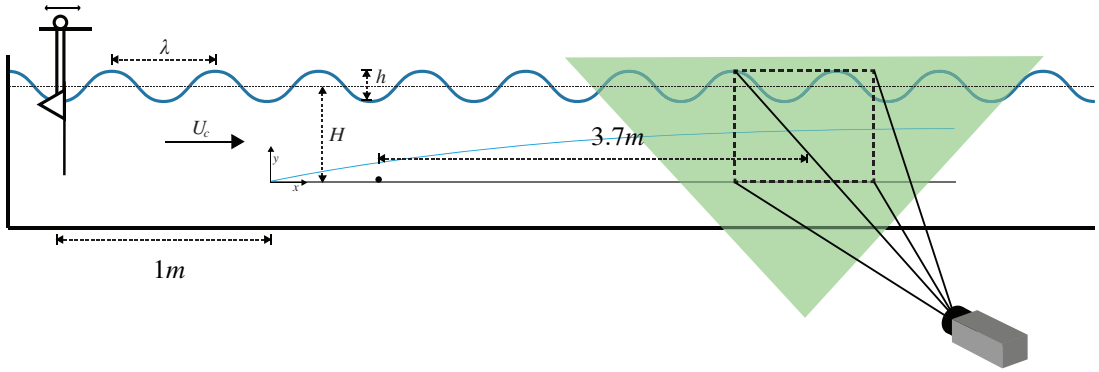

Figure 1: Schematic of bottom boundary layer under free-surface waves and the PIV setup.

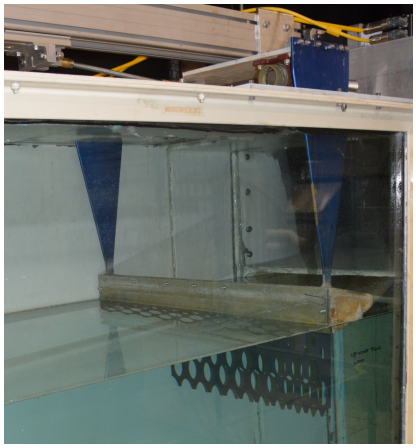

Figure 2: Wave generating paddle that is linearly actuated in the streamwise direction.

mally at NASA Wallops). The experimental apparatus is depicted in Figure 1. The test section of the water channel portion of this facility is 12.2m (40 ft) long with a width of 0.91m and a maximum depth of 0.76m. A boundary layer was generated on a half inch thick plexiglass plate spanning the test section and approximately H=22.5cm below the water surface. For the purposes of the current tests, data was acquired approximately 4m downstream of the leading edge of the plate and 3.7m downstream of a 1.6mm cylindrical trip. The pump frequency was held constant resulting in a flow velocity in the wave-free case of $U_c = 0.38m/s$, and a boundary layer with a 99% thickness, $\delta = 13.5cm$, and a Reynolds number, $Re_\tau = \delta u_\tau/\nu = 2000$ where u_τ is the friction velocity and ν is the kinematic viscosity.

Surface waves were generated using a paddle near the inlet to the test section that was actuated in the streamwise direction in a sinusoidal manner. The wave paddle is shown in Figure 2 and has a triangular section pointing upstream, with a spanwise, perforated plastic sheet attached to its downstream face. This sheet is designed to increase the depth profile of the resulting waves so that they more closely resemble those in shallow water and ensuring a significant velocity perturbation across the water column. At the downstream end of the channel, honeycomb was set on a 45 degree angle to act as a beach to minimize wave reflections.

A schematic of the Particle Image Velocimetry (PIV) setup is also shown in Figure 1. Streamwise/wall-normal two-component velocity fields were acquired using a 1280×1024 pixel Microtron EoSens camera illuminated using a New Wave Solo dual pulse Nd:YAG laser. The approximately 2mm thick laser sheet was generated outside the tunnel, and reached the test location at the mid-span of the test plate from below by reflecting off a 45 degree mirror. The resulting field-of-view was approximately 33cm by 26cm $(2.45\delta \times 2\delta)$ and therefore covered the entire water depth and allowed for examination of the large-scale structure of the boundary layer. Particle images were larger than 2 pixels.

The PIV images were analyzed using a multi-pass cross-correlation algorithm as implemented in PIVlab 1.41 (Thielicke & Stamhuis, 2014). Three passes were used, with initial and final window sizes of 128x128 and 32x32 pixels, respectively. Depending on the case, the interframe time $(10-15ms)$ was set so that maximum particle image displacements were approximately 10 pixels. A normalized median filter with a threshold value of two was used to validate resulting velocity vectors (Westerweel & Scarano, 2005). The resulting vector spacing for the following data was approximately 100 wall units, and so some filtering of small-scale turbulent energy is expected. However, the aim is to investigate the large-scale structure of the boundary layer and so this does not impact the conclusions of this paper.

Image pairs were acquired at a rate of 4Hz while the frequency of the surface waves was chosen to be 2Hz, causing alternating image pairs to match opposite phases of the wave cycle. Only the wave amplitude was varied between sets. Data was acquired for three flows; the unperturbed boundary layer, the wave without mean current, and the boundary layer and surface wave combined. Three wave amplitudes were investigated up to a nominal amplitude of 6cm. A total of 75000 velocity fields were acquired for the wave-free boundary layer, 60000 frames for cases with both the boundary layer and waves and 10000 when examining the waves fields in isolation.

RESULTS AND ANALYSIS

We begin by examining the velocity profiles of the wave-free boundary layer, which was determined to have a 99% thickness, $\delta = 13.5cm$, and a Reynolds number, $Re_\tau = \delta u_\tau/\nu = 2000$. The boundary layer thickness is thus approximately $0.6H$. The mean velocity profile is shown in logarithmic form in Figure 3a, where $U^+ = U/u_\tau$ and $y^+ = yu_\tau/\nu$. The friction velocity, u_τ, was estimated for the wave-free case using the Clauser chart method, that is, by matching a portion of the transformed velocity profile to the log-law with von Kármán constant $\kappa = 0.4$, and additive constant $B = 5.1$.

The wave-free profile is seen to follow the logarithmic slope for almost a full decade before deviating below this slope in the wake region. This is consistent with the presence of a slightly favorable

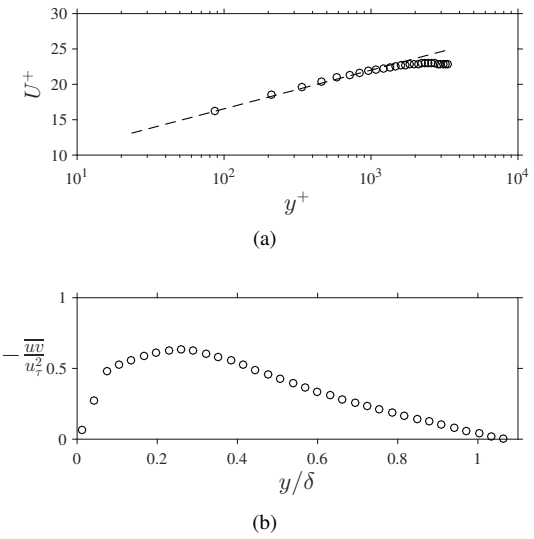

Figure 3: (a) Mean velocity profile and (b) Reynolds shear stress profile for the unperturbed boundary layer.

pressure gradient at the testing location, thought to be due to the side walls of the test section. Alternately, the wake amplitude of the mean velocity profile may be reduced due to the large freestream turbulence level of the current facility (Coles, 1962), which was observed to be upwards of $5\%U_c$.

While the streamwise and wall-normal Reynolds stresses (not shown) reflect the increased disturbance level of the facility, the turbulent shear stress profile, -$\overline{uv}$, of the wave-free cases appears largely unaffected, as shown in figure 3b. The variables u and v are the streamwise and wall-normal velocity fluctuations, respectively and the overbar signifies an ensemble average. The profile follows the expected trend, peaking near the wall at a value less than one and then reducing almost linearly toward zero at the edge of the boundary layer. This would suggest that freestream noise in this facility is uncorrelated in the streamwise and wall-normal directions and therefore has not significantly affected the underlying boundary layer structure. The near-wall peak is lower and further from the wall than that expected for this Reynolds number, indicating some filtering of near-wall small-scale turbulence, as anticipated for the measurement resolution. While a complicating factor, the high freestream turbulence level of the current facility appears to have little effect on the shear stress profile and so the effect on large-scale productive motions, and therefore the conclusions of this paper, is also thought to be minimal.

The boundary layer was examined at a nominally constant current velocity and for three sets of surface waves of increasing amplitude, h. The wave amplitudes were measured to be 2, 4 and 6cm respectively, without a mean current. A sinusoidal profile was iteratively matched to the wall-normal velocity signal of a moving average of 100 frames at each wall-normal location. The median of these fits (which insensitive to any outliers) was used to determine the wavelength, which was approximately 45cm or 3.3δ.

The presence of the surface waves was observed to significantly alter the curvature of the mean velocity profile in the outer layer and toward the free surface as shown in Figure 4. The boundary layer also has a "fuller" profile in the near-wall region. Overall, these changes to the mean velocity profile reflect a reduction in Reynolds number and suggest significant changes to turbulent structure due to the non-linear interaction of the boundary layer and two-dimensional wave perturbations. These results follow the trends observed by Kemp & Simons (1982) for following waves.

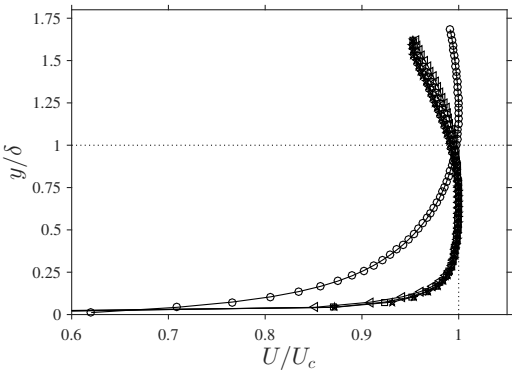

Figure 4: Comparison of mean velocity profile with and without waves. ○ Current only. ◁, Current and wave 1 (W1C). □ Current and wave 2 (W2C). ☆ Current and wave 3 (W3C). Boundary layer thickness for the wave-free case has been used for all profiles.

While the change in mean velocity profile from the wave-free boundary layer to the case with small-amplitude waves is significant, further increasing wave amplitude was observed to only have a minor effect. It was found that while a range of waves amplitudes could be generated in the absence of bottom boundary layer, the difference between each set of waves was significantly reduced once the mean current was introduced and the surface waves developed in conjunction with the boundary layer. As a result, the remainder of the paper will focus on a comparison between the unperturbed boundary layer and the case with the smallest wave amplitude (W1C).

As noted previously, POD has been proven useful for the identification of many coherent structures in turbulent wall-bounded flows, especially those that are reminiscent of hairpin packets and contribute to the majority of the turbulent shear stress and production. We now employ POD to examine changes to the spatial structure of the turbulent boundary layer resulting from surface wave perturbations. POD decomposes the flow into a set of optimal basis functions that maximize the mean square projection of the two-point spatial correlation tensor. Modal functions are therefore weighted by their contribution to the Turbulent Kinetic Energy (TKE) (Holmes *et al.*, 1998). Many versions of POD have been proposed but we choose to employ the method of snapshots of Sirovich (1987) due to the density of spatial data. While modes resulting from the method of snapshots must be interpreted carefully due to the potential for mode mixing (Hellström, 2015), this method has the advantage of reducing calculation requirements for highly resolved spatial data, such as that derived from PIV.

Using this method, the fluctuating velocity field can thus be represented by the sum of the product of the spatial orthogonal eigenmodes, ϕ_n, and their temporal coefficients, a_n, i.e.

$$u(\mathbf{x},t) = \sum_{n=1}^{N} a_n(t)\,\phi_n(\mathbf{x})$$

where n is the mode number and N is the number of snapshots. The determination of these eigenmodes involves the solution to an eigenvalue problem, with significantly greater quantities of data required to converge higher order modes which represent smaller structures. The eigenvalue problem solution also determines the full set of N optimal modes that represent the flow, however many of the higher order modes will necessarily represent measurement noise

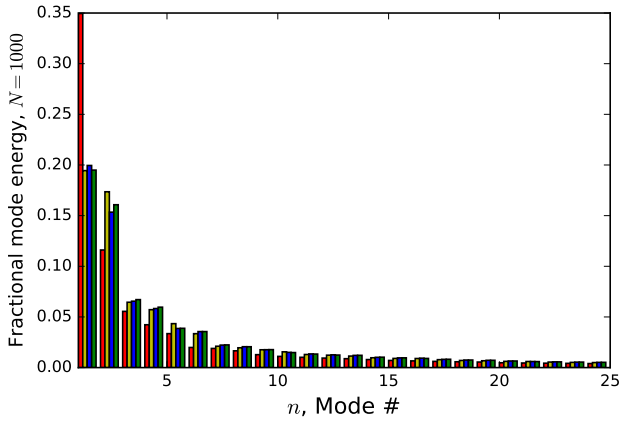

Figure 5: Modal energy content as a fraction of the sum of the energy in the first 1000 POD modes. Red - Unperturbed boundary layer (BL). Yellow - BL and smallest wave. Blue - BL and medium wave. Green - BL and largest wave.

and are therefore not needed. For efficiency we employ a method of randomized sampling Halko *et al.* (2009) to compute only a limited number low-order modes of interest, using an approximation to the full variation of the data.

The randomized Principle Component Analysis (PCA) method available in the Python Scikit-Learn package (and equivalent to snapshot POD) was used for to obtain an approximation to the first 1000 orthogonal modes for the flow with and without waves. As an example of the benefits of this approach, this calculation could be accomplished on the 75000 frame dataset in approximately 3 minutes, whereas the full solution was not possible due to memory limitations. Comparisons were made between the randomized and full eigenvalue solutions for subsets of the data and the resulting modal structures could not be distinguished. The energy content of each mode as a fraction of the cumulative energy in the first 1000 modes is shown in figure 5 for all four cases. As with the mean velocity profiles, the modal energies for each of the perturbed cases is very similar and so we shall focus on the case with the smallest wave amplitudes (W1C).

The turbulent energy is distributed over a range of lengthscales and so we choose to examine the structure of the first thirty modes in each case. Normalized modes for the wave-free case are shown in figure 6a, focussing on the region of the flowfield within the turbulent boundary layer. A wide range of inclined, attached low and high streamwise-momentum structures are observed, a subset of which are highlighted with yellow boxes. The lengthscale of these structures is seen to decrease with increasing wavenumber. The largest of these modes has a streamwise lengthscale on the order of field of view or 2.5δ. Upon examination of the wall-normal modes, it is clear that these structures predominantly contribute to a negative turbulent shear stress and thus positive turbulent production.

For this reason, we begin by searching for similar structures in the perturbed boundary layer, whose modes are shown in figure 6b. As noted previously, the modes for the other two wave amplitudes depict very similar structures. The first three perturbed boundary layer modes clearly indicate a streamwise periodicity indicative of the surface wave motion. Inclined attached structures are still present but they are less distinct in most cases. While the first of these structures appears in the fourth mode, as in the unperturbed boundary layer case, the perturbed mode has a shorter streamwise lengthscale, less than the wavelength of the surface waves. Additionally, the angle of inclination of these structures is seen to be increased in comparison with the wave-free case, likely in response to wall-normal component of the wave-field. Further comparison between the two cases suggests that detached structures are also more vertical in nature.

These results suggest that the largest-scale productive motions of the turbulent boundary layer are significantly altered when of the same size or greater than the wavelength of the surface wave disturbance. The waves appear to have less effect on smaller-scale structures.

CONCLUSIONS

Large PIV datasets were acquired to examine changes to the spatial structure of turbulent boundary layers in the presence free-surface waves. These large datasets were necessary to converge spatial POD modes to sufficiently high order, so that a range of turbulent lengthscales and productive motions could be examined. For the current experiments the wavelength was approximately three times the boundary layer thickness. While a hierarchical series of inclined low- and high-momentum structures, reminiscent of hairpin packets, are observed near to the wall in for both wave-free and perturbed cases, these structures are observed to be highly disrupted by the depth-varying wave perturbation. Fewer of these structures were observed when waves were present. Those that remained were inclined at a greater angle and were weaker, relative to other structures visible in the POD modes. Perhaps most significantly, the largest such inclined structure was found to have a streamwise lengthscale less than that of the wavelength of the disturbance, suggesting that surface waves significantly disrupt the largest productive motions of sizes equal to or greater than the wavelength. Further experiments are required to determine if this result holds for a wider range of wavelengths or if the small-scale structures are less influenced by the surface waves because of the innate weakening of the wave motions near the wall.

REFERENCES

Borue, Vadim, Orszag, Steven A. & Staroselsky, Ilya 1995 Interaction of surface waves with turbulence: direct numerical simulations of turbulent open-channel flow. *Journal of Fluid Mechanics* **286**, 1–23.

Calmet, Isabelle & Magnaudet, Jaques 2003 Statistical structure of high-reynolds-number turbulence close to the free surface of an open channel. *Journal of Fluid Mechanics* **474**, 355–378.

Coles, D. 1962 The turbulent boundary layer in a compressible fluid. *Tech. Rep.*. Report R-403-PR, The Rand Corporation, Santa Monica, California.

Halko, N., Martinsson, P. G. & Tropp, J. A. 2009 Finding structure with randomness: Stochastic algorithms for constructing approximate matrix decompositions. *arXiv: 0909.4061* .

Hellström, Leo H.O. 2015 Coherent structures in turbulent pipe flow. PhD thesis, Princeton University.

Hellström, Leo H.O., Ganapathisubramani, B. & Smits, A. J. 2015 The evolution of large-scale motions in turbulent pipe flow. *Journal of Fluid Mechanics* **779**, 701–715.

Hellström, Leo H.O., Marusic, Ivan & Smits, Alexander J. 2016 Self-similarity of the large-scale motions in turbulent pipe flow. *Journal of Fluid Mechanics* **792**.

Holmes, P., Lumley, J. L., Berkooz, G. & Rowley, C.W. 1998 *Turbulence, coherent structures, dynamical systems and symmetry*. Cambridge University Press.

Hussain, A.K.M.F. & Reynolds, W.C. 1970 The mechanics of an organized wave in turbulent shear flow. *Journal of Fluid Mechanics* **41**, 241–258.

Kemp, P.H. & Simons, R.R. 1982 The interaction between waves

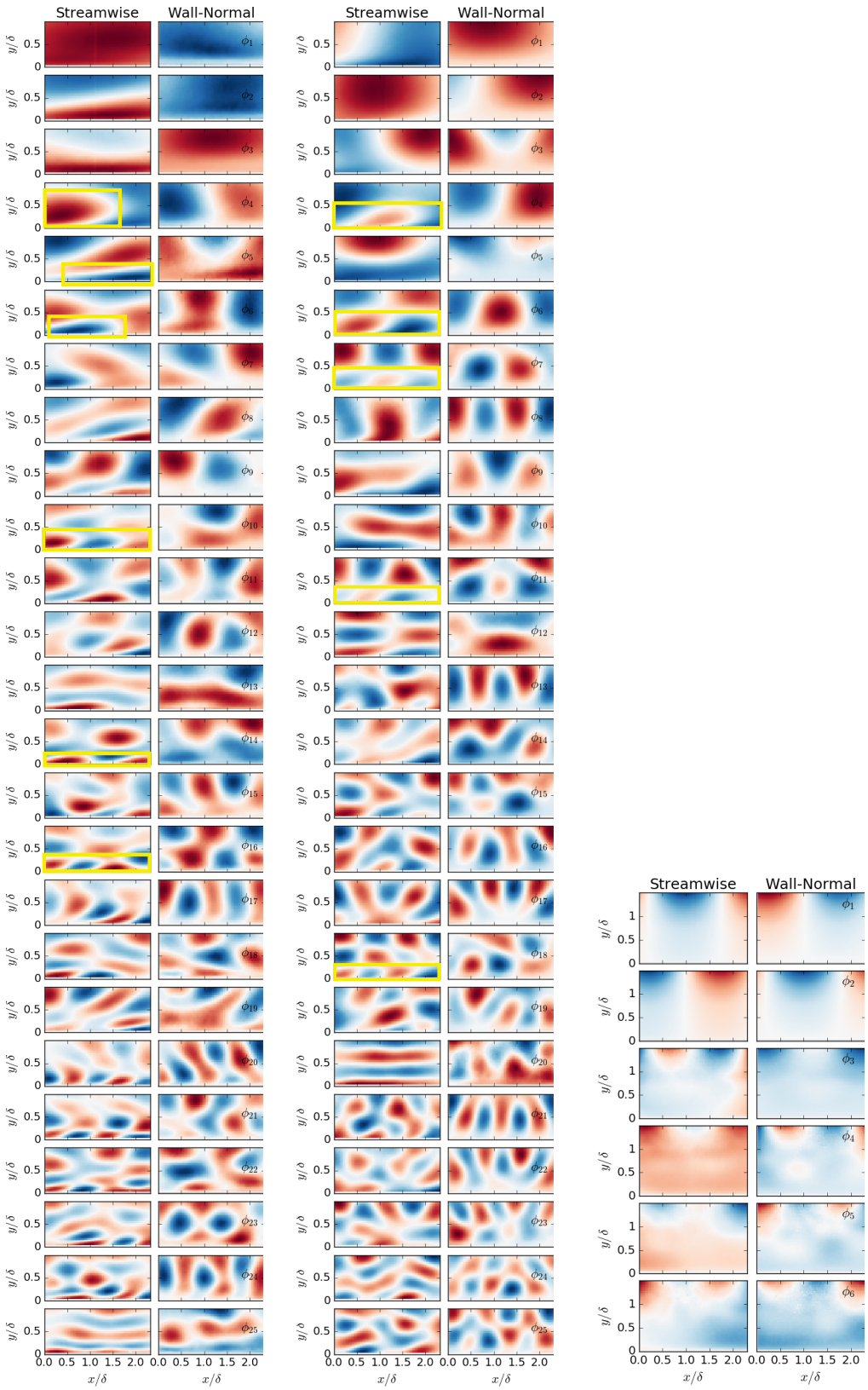

(a) (b) (c)

Figure 6: First 25 POD modes in the streamwise and wall-normal directions for the (a) unperturbed boundary layer (C) and (b) boundary layer with waves (W1C). (c) The first six POD for the waves alone (W1), where 95% of the energy is in the first two modes. Increasing mode number from top to bottom. Red and blue indicate positive and negative velocity fluctuations . Yellow boxes highlight a some of the inclined, attached near-wall regions of high and low momentum fluid that contribute to the turbulent shear stress.

and a turbulent current : waves propagating with the current. *Journal of Fluid Mechanics* **116**, 227–250.

Kemp, P.H. & Simons, R.R. 1983 Ther interaction of waves and a turbulent current: waves propagating against the current. *Journal of Fluid Mechanics* **130**, 73–89.

Sirovich, L. 1987 Turbulence and the dynamics of coherent structures. part 1: Coherent structures. *Quarterly of Applied Mathematics* **45**, 353–375.

Smits, A. J. & Wood, D. H. 1985 The response of turbulent boundary-layers to sudden perturbations. *Annual Review of Fluid Mechanics* **17**, 321–358.

Thielicke, W. & Stamhuis, E.J. 2014 Pivlab - time-resolved digital particle image velocimetry tool for matlab (version: 1.41). *http://dx.doi.org/10.6084/m9.figshare.1092508* .

Umeyama, M. 2005 Reynolds stresses and velocity distributions in a wave-current coexisting environment. *Journal of waterway, port, coastal and ocean engineering* **131** (5), 203–212.

Westerweel, J. & Scarano, F. 2005 Universal outlier detection for PIV data. *Experiments in Fluids* **39** (6), 1096–1100.